Dual-Functional Fe_3O_4@SiO_2/Ag/AgCl Nanocomposites as Photocatalyst for Degrading Methylene Blue Dye Under Natural Light Irradiation

Kha Minh Nguyen[1,2*], Nga Ngan Pham[1,2], Hien Thi-Thu Tran[1,2], and Son Truong Nguyen[1,2]

[1]*Faculty of Chemical Engineering, Ho Chi Minh City University of Technology (HCMUT), 268 Ly Thuong Kiet St., Dist. 10, Ho Chi Minh City 700000, Vietnam*

[2]*Vietnam National University Ho Chi Minh City, Linh Trung Ward, Thu Duc Dist., Ho Chi Minh City 700000, Vietnam*

* ***Corresponding author:***

email: nmkha@hcmut.edu.vn

Received: August 14, 2024
Accepted: October 7, 2024

DOI: 10.22146/ijc.99129

Abstract: *The textile dyeing industry not only plays a crucial economic role in many nations but also significantly contributes to environmental pollution, particularly in aquatic environments. To mitigate this impact, various materials have been explored for their ability to remove dyes from wastewater. Among these, visible-light-responsive photocatalysts based on Ag nanomaterials have attracted considerable attention. However, challenges remain, including the degradation efficiency and the recoverability of photocatalysts. In this study, Fe_3O_4@SiO_2/Ag/AgCl (FSAC) nanocomposites were synthesized and evaluated for methylene blue (MB) dye degradation under natural light irradiation. The magnetic properties of FSAC remained those of the core Fe_3O_4 nanoparticles, with a band gap energy of approximately 1.8 eV. Results showed that the photocatalytic decomposition of MB under 25 W natural light was significantly enhanced in the presence of the FSAC nanocomposites, compared to Fe_3O_4, Fe_3O_4@SiO_2, and Fe_3O_4@SiO_2/Ag nanoparticles. With its dual-functional magnetic and plasmonic properties, enabling both efficient recovery and superior catalytic performance, the FSAC composite holds excellent promise as a photocatalyst for the degradation of organic pollutants in water.*

Keywords: *dye removal; surface plasmon; core-shell; photocatalyst; Ag nanoparticle*

■ INTRODUCTION

Dyes and organic pigments are among the most common pollutants in industries such as textile, leather, paper, cosmetics, paint, and printing. Textile dyes, in particular, often contain many toxic organic ingredients discharged into rivers, causing risks to soil, groundwater, and aquatic microorganisms [1]. Methylene blue (MB, $C_{16}H_{18}ClN_3S$), an azo dye (–N=N–), is widely used in laboratories and industries [2]. Due to its stable structure, dye-contaminated wastewater is difficult to decompose under natural conditions, potentially causing harmful effects on human health, including skin irritation, kidney dysfunction, and even cancer. The treatment of wastewater containing organic dyes has become a critical area of research. Photocatalysis, a modern green chemical technology, uses sunlight to conduct oxidation reactions that decompose organic pollutants [3], making it a promising approach for the removal of dyes from wastewater.

The surface plasmon resonance (SPR) effect of silver (Ag) significantly enhances photocatalytic activity through hot electron injection [4-5]. Ag nanoparticles (NPs), especially in Cl^- ion environments, tend to partly convert into AgCl [6], a known photoactive material. Silver halides (AgX, where X is Cl, Br, I) have gained attention as photosensitizers in the past decade. Although their high photosensitivity suggests photocatalysis potential, a continuous reduction of Ag^+ to Ag^0 under light undermines their stability and lifetime. Methods like introducing Ag_3PO_4 as support [7] or combining with BiOX (where X is Cl, Br) [8] have been explored to improve the photocatalytic efficiency and stability of AgX. However, these often require complex processes and harsh conditions. The SPR effect in Ag/AgX systems is particularly noted for its role in

accelerating dye photodegradation, with Ag/AgCl demonstrating rapid kinetics and high efficiency [9]. However, challenges remain, such as the separation of nanocatalysts and the mitigation of their release as a secondary pollutant.

Conventional separation methods, including centrifugation and filtration, often lead to significant catalyst loss as well as high energy consumption. To address this issue, immobilizing photocatalysts on thin films is considered a valuable option [10], though it typically reduces photochemical efficiency due to the decreased active surface area. Another approach involves coating catalysts on monolith tubes to aid in recovery [11]. However, the frame material, such as the monolith tube, limits light transmission to the catalyst layer inside. Therefore, designing a photocatalytic system that balances high activity, cost-effectiveness, and ease of separation remains a significant challenge.

To solve the challenge of nanocatalyst separation, magnetic photocatalysis has garnered significant attention in recent research [12-13]. Magnetic iron oxide (Fe_3O_4) is particularly appealing in composite materials due to its non-toxic nature and strong magnetic responsiveness, allowing easy separation from treated water using an external electromagnetic field. Combining Fe_3O_4 particles with photocatalytic NPs offers the advantage of environmental friendliness and ease of recovery. In addition, the catalyst layer on Fe_3O_4 helps prevent the aggregation of catalyst particles. However, Fe_3O_4 NPs are less stable under photochemical conditions, and direct attachment to photocatalytic NPs accelerates electron-hole recombination [14], leading to a rapid decline in photocatalytic activity.

In this study, Fe_3O_4 is coated with a SiO_2 layer, acting as a barrier between the magnetic core and the Ag/AgCl photocatalytic shell. This design minimizes the negative effects of Fe_3O_4 on the photochemical process while protecting the magnetic core and improving catalyst recovery efficiency. Moreover, Ag/AgCl is a highly photosensitive material, particularly active in the visible light spectrum. The photocatalysis performance of Fe_3O_4@SiO_2/Ag/AgCl (FSAC) nanocomposites for MB degradation was evaluated under natural light irradiation.

■ EXPERIMENTAL SECTION

Materials

Iron(III) chloride hexahydrate ($FeCl_3{\cdot}6H_2O$, 99%), iron(II) chloride tetrahydrate ($FeCl_2{\cdot}4H_2O$, 99%), ethanol (C_2H_5OH, 99.5%), and ammonium hydroxide solution (NH_4OH, 28%) were purchased from Shanghai reagent factory. The MB, ($C_{16}H_{18}ClN_3S$, ≥ 98%), (3-aminopropyl)triethoxysilane (APTES, $H_2N(CH_2)_3Si(OC_2H_5)_3$, ≥ 98%), sodium borohydride ($NaBH_4$, 98%), tetraethyl orthosilicate (TEOS, $Si(OC_2H_5)_4$, 98%), silver nitrate ($AgNO_3$, 99%), and polyvinylpyrrolidone (PVP, $(C_6H_9NO)_n$, Mw = 40,000 g/mol) were sourced from Alfa Aesar. All reagents were of analytical grade and used without further purification.

Instrumentation

The morphology of the nanocomposites was examined using a transmission electron microscope (TEM, JEM-2100), operating at 80 kV. X-ray powder diffraction (XRD) patterns were recorded with a Bruker Advance D8 diffractometer. UV-visible diffuse reflectance spectroscopy (UV-vis DRS) data were obtained with a Jasco V-750 UV-vis spectrophotometer. The magnetic properties were characterized with a vibrating specimen magnetometer (VSM). The presence of elements in the nanocomposite was analyzed with a scanning electron microscope (SEM) and energy dispersive X-ray spectroscopy (EDS) JSM-IT200 JEOL.

Procedure

Fe_3O_4 NPs preparation

Fe_3O_4 (F) NPs were synthesized via the coprecipitation method using Fe^{2+} and Fe^{3+} ions. A solution with a Fe^{2+}/Fe^{3+} molar ratio of 1:2 was prepared by dissolving 6.5 g $FeCl_3{\cdot}6H_2O$ and 2.9 g $FeCl_2{\cdot}4H_2O$ in 400 mL of distilled water, then heating it to 50 °C. Subsequently, 18 mL of NH_4OH was slowly added under vigorous stirring for 15 min. The NPs were magnetically separated, washed with water and ethanol, and dried at 50 °C for 3 h.

Fe_3O_4@SiO_2 NPs preparation

Fe_3O_4@SiO_2 (FS) core-shell NPs were synthesized using the Stöber method. The synthesized F NPs were dispersed in a mixture of ethanol (60 mL), NH_4OH (10 mL), and distilled water (15 mL). TEOS solution (0.02 M) was added dropwise under continuous stirring. After 2 h, the FS NPs were magnetically separated, washed with water and ethanol, and dried at 50 °C for 3 h.

Fe_3O_4@SiO_2/Ag NPs preparation

To enhance the interaction between FS and Ag, 1.2 g of FS NPs were dispersed in a solution containing ethanol (40 mL) and distilled water (15 mL). A solution of 250 µL of APTES dissolved in 12.5 mL of ethanol was then added. After 2 h, the FS-APTES NPs were collected. Next, 1.2 g of FS-APTES was dispersed into $NaBH_4$ solution (100 mL, 0.02 M), and $AgNO_3$ (10 mL, 0.1 M) was dropped. The resulting Fe_3O_4@SiO_2/Ag sample (FSA) was washed with water.

Fe_3O_4@SiO_2/Ag/AgCl NPs preparation

To synthesize FSAC, 0.5 g of FSA was dispersed in 30 mL of water. Then, 80 mg of PVP was added, and the mixture was stirred for 30 min. The investigated amount of $FeCl_3$ (0.1 M) was added dropwise to the solution. After 2 h, the sample was washed with ethanol and water and dried in the dark. To evaluate the photocatalytic activity of the synthesized NPs, 200 mg of catalyst was suspended in 200 mL of a 10 ppm MB solution. After stirring the solution in the dark for 90 min, the solution was exposed to 25 W natural light (Exo Terra). At 30-min intervals during irradiation, 2 mL of the solution was sampled and filtered through a 0.45 µm membrane filter. The MB concentration was then measured using a Jasco V-730 UV-vis spectrophotometer.

■ RESULTS AND DISCUSSION

Material Characterization

To confirm the crystalline phases present in the nanocomposites, XRD patterns of FS and FSAC samples are shown in Fig. 1. The diffraction peaks observed in the FS sample correspond to the (220), (311), (400), (422), (511), and (440) planes of the spinel Fe_3O_4 structure (JCPDS card no. 85-1436). In the XRD pattern of FSAC, the main peaks of Fe_3O_4 are clearly identified. Besides that, prominent diffraction peaks at 2θ values of 38.3, 44.5, and 64.6° in the FSAC sample are attributed to Ag (JCPDS card no. 4-0783). However, distinct diffraction peaks for AgCl are absent in the XRD pattern of FSAC, likely due to its low content, high dispersity, or low crystallinity. The EDS analysis (Fig. 2) confirms the presence of Ag and Cl elements, verifying the formation of Ag/AgCl within the dual-functional FSAC nanocomposite.

The TEM image of the F sample (Fig. 3(a)) reveals that the sample consists of numerous spherical particles with an average diameter of ~18 nm. After coating with SiO_2, Ag, and AgCl, the FSAC NPs were well dispersed, clearly displaying the core-shell structure (Fig. 3(b)). The SiO_2/Ag/AgCl shell is uniform, with a thickness of ~2.5 nm (Fig. 3(c)). The improved dispersity of FSAC NPs

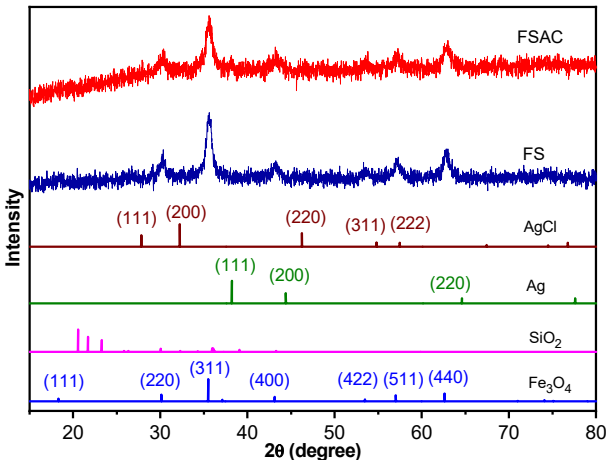

Fig 1. XRD patterns of FS and FSAC

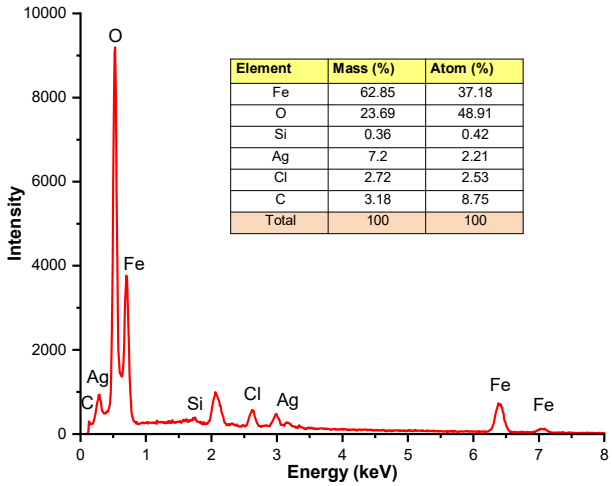

Fig 2. EDS analysis of FSAC nanocomposite

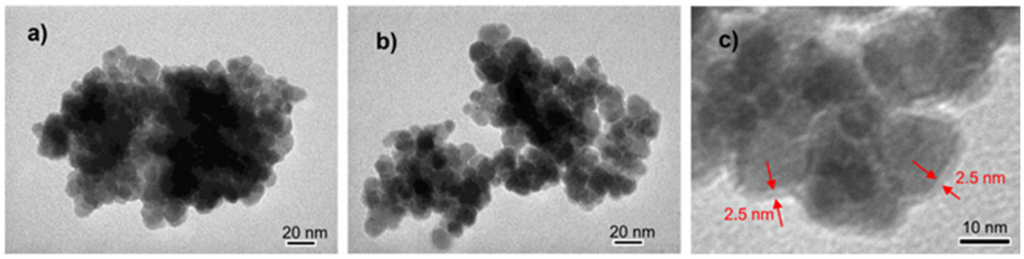

Fig 3. TEM images of (a) F and (b and c) FSAC

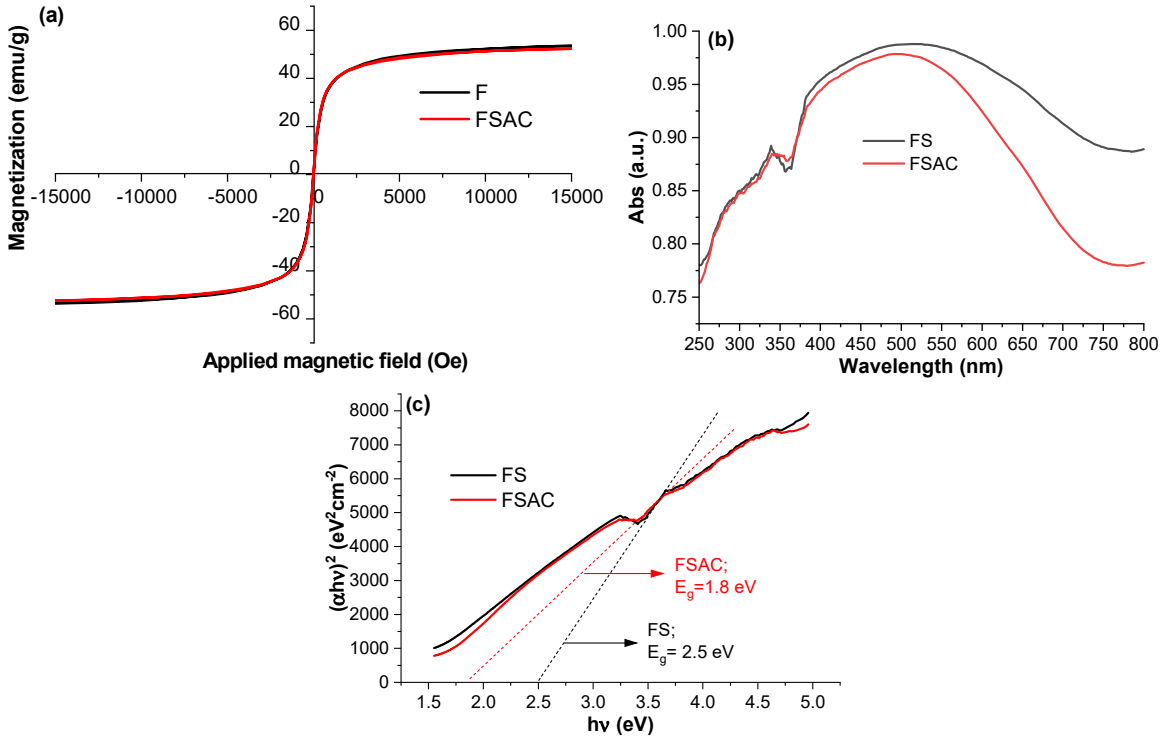

Fig 4. (a) Magnetization curves of F and FSAC, (b) UV-vis DRS, and (c) band gap energy of FS and FSAC

confirms that the SiO_2/Ag/AgCl shell effectively reduces the aggregation of Fe_3O_4 NPs. VSM was used to assess the magnetic properties of F and FSAC materials in Fig. 4(a), indicating that both materials exhibit superparamagnetic properties. The saturation magnetization values for F and FSAC are 53.5 and 52.4 emu/g, respectively. The slight decrease in saturation magnetization in the FSAC sample can be attributed to the presence of a SiO_2 coating surrounding the Fe_3O_4 core, along with layers of Ag and AgCl NPs. However, this reduction is minimal, suggesting that the adhesion of Ag and AgCl NPs has a negligible impact on the magnetism of the Fe_3O_4 core when a thin SiO_2 coating is coated. These results demonstrate that, despite multiple layers, the FSAC core-shell structure retains strong magnetic properties, facilitating easy separation and recovery from solutions. Additionally, UV-vis DRS was used to evaluate the optical properties (Fig. 4(b)), which are influenced by the SPR of Ag NPs. It is well known that Schottky barriers and SPR occur at the interface between metal and semiconductor materials [15], and the addition of Ag/AgCl can further enhance photocatalytic activity [16]. Fig. 4(c) illustrates the relationship between photon energy (hν) and light absorption (αhν), calculated using the Tauc formula [17]. The band gaps of FS and FSAC are determined by the equation Eq. (1);

$$(\alpha h\nu)^2 = A\left(h\nu - E_g\right) \quad (1)$$

where α is the absorption coefficient (cm^{-1}), h is Planck's constant, ν is the frequency of the incident photon, A is

a constant related to the degree of band tailing, and E_g represents the band gap energy (eV). Previous research has established the E_g of Fe_3O_4 NPs to be 2.12 eV [18]. When these Fe_3O_4 NPs are coated with a thin layer of SiO_2, an insulating material, the E_g of the resulting FS material increases to 2.5 eV, which aligns with expectation. Notably, when Ag and AgCl NPs are incorporated onto the FS surface, the E_g of FSAC decreases significantly to 1.8 eV due to the SPR effect of Ag NPs, consistent with the previous reports [19-20]. This decline in E_g indicates a substantial enhancement in the photocatalytic properties under natural light irradiation of FSAC compared to FS. Collectively, these characterization techniques confirm the successful synthesis and multifunctional properties of the FSAC nanocomposites.

Photocatalytic Performance

The photocatalytic activity of FSAC nanocomposite was investigated by varying the $FeCl_3$:$AgNO_3$ ratios. The MB degradation under natural light irradiation served as the benchmark for evaluating performance. Fig. 5(a) illustrates that by the end of the experiment, the remaining MB concentration relative to the initial concentration for the samples FSAC-1:4, FSAC-1:2, FSAC-1:1, FSAC-2:1, and FSAC-4:1 was 82.1, 85.7, 54.8, 51.8, and 74.4%, respectively. Consequently, these samples' corresponding MB dye treatment efficiencies were 17.9, 14.3, 45.2, 48.2, and 25.6%, respectively. As the $FeCl_3$:$AgNO_3$ ratio increases, the photocatalytic activity gradually improves from 1:2 to 2:1 (rising from 17.9% to 48.2%). However, the activity decreases when the ratio shifts to 4:1 (dropping to 25.6%), indicating that photocatalytic efficiency depends heavily on the amount of AgCl and Ag on the FSAC's surface. The likely explanation for this trend is that increasing the $FeCl_3$:$AgNO_3$ ratio during preparation leads to more Ag being oxidized to form AgCl crystal. The additional AgCl on the surface of Ag NPs helps prevent the recombination of electron-hole pairs [21], thereby stabilizing the SPR phenomenon of the Ag NPs (Fig. 5(b)). This stabilization enhances the efficiency of the photocatalytic process. However, when the $FeCl_3$ amount becomes too high, excessive AgCl formation reduces the amount of free Ag in the catalyst, weakening the SPR and leading to a decline in photocatalytic efficiency. Based on the results, the FSAC NPs prepared with a $FeCl_3$:$AgNO_3$ ratio of 2:1 exhibited the highest photocatalytic efficiency due to enhanced light absorption, minimized electron-hole recombination, and increased production of reactive species such as hydroxyl radicals (•OH) and superoxide anions (O_2•$^-$).

The photocatalytic performance of FSAC nanocomposite was evaluated at different dosages to determine the optimal amount required for maximum efficiency in degrading MB. As presented in Fig. 6(a), increasing the dosage from 0.5 to 1.0 g/L enhanced the decomposition efficiency of MB from 30.3% to 48.2%. However, further increasing the dosage to 1.5 g/L decreased treatment efficiency to 28.6%. Initially, the increase in catalyst quantity amplifies the number of

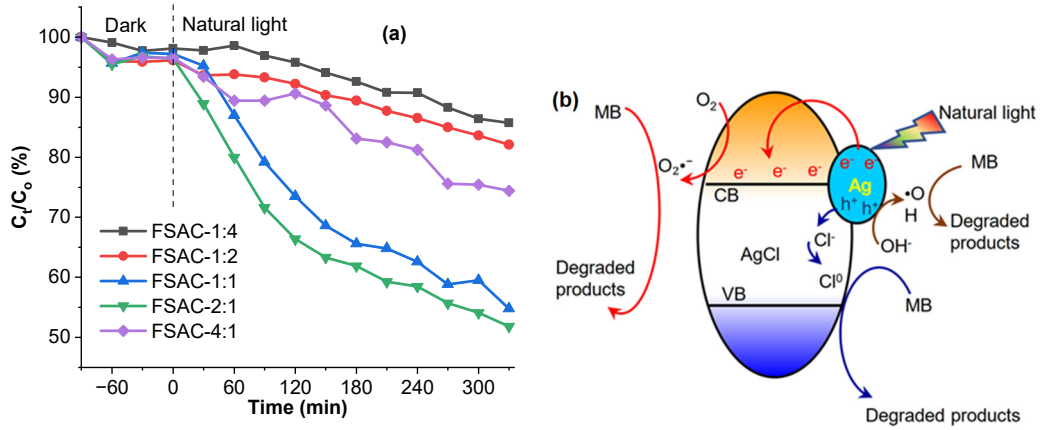

Fig 5. (a) Photocatalytic activity of FSAC composites prepared by varying the $FeCl_3$:$AgNO_3$ ratios. (b) Schematic illustration of the movement of electrons-holes as well as their reactions on the contact surface of Ag/AgCl

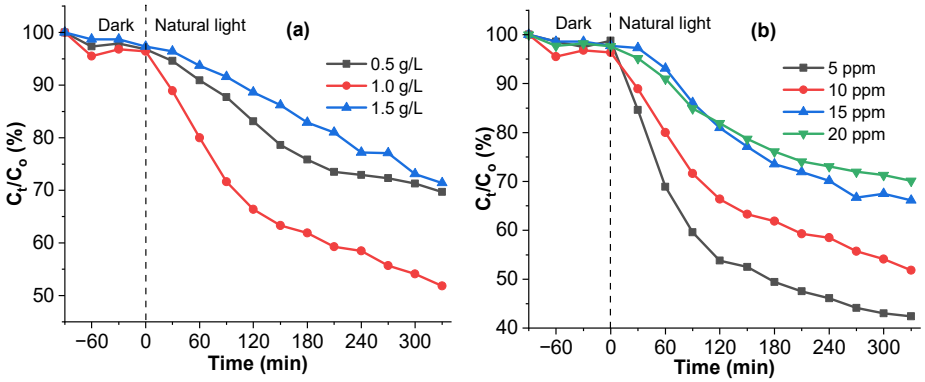

Fig 6. Photocatalytic activity of FSAC-2:1 with (a) different dosages and (b) different MB concentrations

active sites on the photocatalyst surface, providing a greater rate of electron-hole pair generation and improving MB decomposition efficiency. Insufficient catalyst amounts result in fewer available active sites, leading to lower reaction rates for the degradation of pollutants.

At higher dosages, however, the photocatalytic activity does not increase proportionally and, in some cases, declines. This trend can be attributed to the balance between catalyst surface area and light absorption [22]. Increasing the catalyst quantity raises turbidity and light scattering in the solution, reducing light penetration and limiting the activation of the SPR in Ag NPs. Additionally, excessive catalyst amount can lead to particle aggregation, reducing the effective surface area and the number of active sites, thereby lowering photocatalytic efficiency. Identifying and maintaining the optimal dosage is crucial for maximizing the efficiency of these nanocomposites in environmental remediation, particularly in the degradation of organic pollutants. Based on these observations, a dosage of 1 g/L was determined to be optimal for the photochemical decomposition of MB using the FSAC-2:1 catalyst. This dosage will be used in subsequent experiments.

The initial concentration of the dye solution is another crucial factor requiring investigation. Fig. 6(b) presents the results on the effect of the initial MB concentration, showing that the percentage of MB remaining after treatment for initial concentrations of 5, 10, 15, and 20 ppm were 42.4, 51.8, 66.1, and 70.1%, respectively. These results clearly indicate that the photochemical decomposition efficiency improves as the initial dye concentration decreases. At lower concentrations, the excess availability of active sites on the nanocomposites relative to the number of MB molecules ensured efficient adsorption and degradation. To further clarify this relationship, the total moles of MB processed per gram of catalyst are also considered. During the adsorption stage in the dark, it was observed that as the initial concentration increased from 5 to 20 ppm, the total moles of MB processed per gram of catalyst also increased. This outcome is expected, as a higher initial concentration means more dye molecules are present and available to be adsorbed onto the catalyst surface. A similar trend was observed during the initial stage of the photochemical process, where more MB molecules were photodegraded at higher initial concentrations. However, at higher MB concentrations, the active sites on the FSAC nanocomposite become saturated, leading to a reduction in photocatalytic efficiency. Additionally, higher dye concentrations can result in intermediate degradation products' formation, complicating the pollutant's complete breakdown. These intermediate products and the remaining MB molecules absorb significant amounts of light energy, further decreasing photochemical efficiency. For optimal photocatalytic degradation, it is essential to maintain MB concentrations within a range that ensures efficient interaction with the active sites on the nanocomposites.

Experiments on the degradation of MB were conducted using various materials, including F, FS, FSA, and FSAC, to assess their efficacy as photocatalysts. As shown in Fig. 7, the treatment efficiencies of MB, ranked in descending order, were FSAC (48.2%), FSA (19.6%),

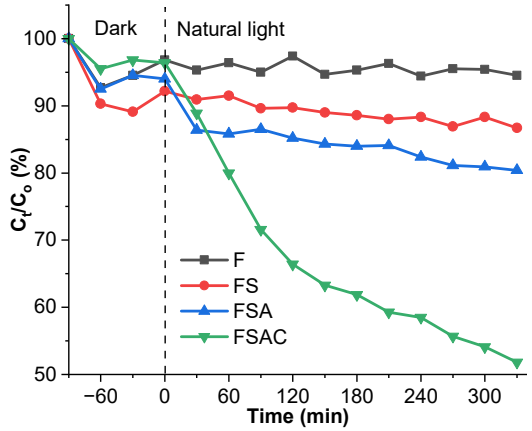

Fig 7. Photocatalytic activity of different catalytic materials under natural light irradiation (dosage of 1 g/L and 10 ppm MB)

FS (13.3%), and F (5.5%). The superior adsorption capacity of FS during the 90-min dark stage can be attributed to the MB adsorption onto the SiO_2 shell. During the photochemical stage, F and FS exhibited no significant photocatalytic capabilities, with their performance limited to adsorption and desorption processes, resulting in minimal treatment efficiencies of 5.5 and 13.3%, respectively. In contrast, FSA and FSAC demonstrated notable photocatalytic performance. With FSA, an initial rapid decrease in MB concentration was observed, followed by a slower decline, likely due to the instability of the Ag NPs, which led to rapid recombination of electron-hole pairs and diminished photocatalytic efficacy. Remarkably, FSAC, incorporating both Ag and AgCl NPs, exhibited a more consistent SPR phenomenon, ensuring a steady and gradual decrease in MB concentration throughout the photochemical process, as presented in Fig. 7. These results indicate that the SiO_2 layer influences the adsorption capacity of the FSAC, while its photocatalytic efficiency is the result of the interaction between Ag and AgCl. It confirmed that FSAC nanocomposites exhibit superior photocatalytic activity compared to individual components such as F, FS, and FSA. This enhanced performance can be attributed to the synergistic effect of its components and the unique core-shell structure, which promotes efficient charge separation and transfer. During photocatalysis, Ag NPs act as electron sinks (as shown in Fig. 5(b)), reducing the recombination rate of photogenerated electron-hole pairs. Additionally, the plasmonic effect of Ag NPs enhances light absorption, increasing the generation of reactive species such •OH and $O_2•^-$. AgCl NPs further contribute by generating electron-hole pairs upon light irradiation, while the Fe_3O_4 core provides magnetic properties, allowing easy recovery of the nanocomposites after the reaction.

■ CONCLUSION

The synthesis of FSAC nanocomposites involves a controlled multi-step process to achieve a core-shell structure with enhanced photocatalytic properties. The optimal condition requires a balanced $FeCl_3$·$AgNO_3$ ratio, which regulates the distribution of Ag and AgCl NPs on the Fe_3O_4@SiO_2 core, preventing aggregation and maximizing the active photocatalytic surface. The photocatalytic activity of FSAC was evaluated under natural light using MB as a model organic pollutant. The results demonstrated that FSAC exhibit superior photocatalytic performance, attributed to their components' synergistic effects. The Fe_3O_4 core provides magnetic properties for easy recovery, the SiO_2 shell prevents recombination of electron-hole pairs, and the Ag/AgCl NPs enhance light absorption and generate reactive species. FSAC nanocomposites synthesized under optimal conditions demonstrated excellent photocatalytic efficiency, making them promising candidates for environmental remediation. The balance of synthesis parameters, pollutant concentrations, and dosages is crucial for maximizing the degradation of organic dyes. This study provides valuable insights into the synthesis and application of FSAC for wastewater treatment and other environmental applications.

■ ACKNOWLEDGMENTS

This research is funded by Vietnam National University Ho Chi Minh City (VNU-HCM) under grant number C2024-20-20.

■ CONFLICT OF INTEREST

The authors declare that there are no conflicts of interest regarding the publication of this paper.

■ AUTHOR CONTRIBUTIONS

Kha Minh Nguyen did conceptualization, methodology, writing, and revising of the manuscript. Nga Ngan Pham and Hien Thi-Thu Tran conducted the experiment. Son Truong Nguyen conducted methods and validation. All authors agreed to the final version of this manuscript.

■ REFERENCES

[1] Dutta, S., Adhikary, S., Bhattacharya, S., Roy, D., Chatterjee, S., Chakraborty, A., Banerjee, D., Ganguly, A., Nanda, S., and Rajak, P., 2024, Contamination of textile dyes in aquatic environment: Adverse impacts on aquatic ecosystem and human health, and its management using bioremediation, *J. Environ. Manage.*, 353, 120103.

[2] Oladoye, P.O., Ajiboye, T.O., Omotola, E.O., and Oyewola, O.J., 2022, Methylene blue dye: Toxicity and potential elimination technology from wastewater, *Results Eng.*, 16, 100678.

[3] Chen, D., Cheng, Y., Zhou, N., Chen, P., Wang, Y., Li, K., Huo, S., Cheng, P., Peng, P., Zhang, R., Wang, L., Liu, H., Liu, Y., and Ruan, R., 2020, Photocatalytic degradation of organic pollutants using TiO_2-based photocatalysts: A review, *J. Cleaner Prod.*, 268, 121725.

[4] Sun, Q., Hou, P., Wu, S., Yu, L., and Dong, L., 2021, The enhanced photocatalytic activity of Ag-Fe_2O_3-TiO_2 performed in Z-scheme route associated with localized surface plasmon resonance effect, *Colloids Surf., A*, 628, 127304.

[5] Gai, Q., Ren, S., Zheng, X., Liu, W., and Dong, Q., 2022, Enhanced photocatalytic performance of Ag/CdS by L-cysteine functionalization: Combination of introduced co-catalytic groups and optimized injection of hot electrons, *Appl. Surf. Sci.*, 579, 151838.

[6] Yang, Y., Wang, K., Liu, X., Xu, C., You, Q., Zhang, Y., and Zhu, L., 2024, Environmental behavior of silver nanomaterials in aquatic environments: An updated review, *Sci. Total Environ.*, 907, 167861.

[7] Wei, X., Yu, F., Ji, J., Cai, Y., Zou, W., Zheng, Y., Huang, J., Zhang, Y., Yang, Y., Naushad, M., Gao, B., and Dong, L., 2021, Porous biochar supported Ag_3PO_4 photocatalyst for "two-in-one" synergistic adsorptive-photocatalytic removal of methylene blue under visible light irradiation, *J. Environ. Chem. Eng.*, 9 (6), 106753.

[8] Arumugam, M., Natarajan, T.S., Saelee, T., Praserthdam, S., Ashokkumar, M., and Praserthdam, P., 2021, Recent developments on bismuth oxyhalides (BiOX; X = Cl, Br, I) based ternary nanocomposite photocatalysts for environmental applications, *Chemosphere*, 282, 131054.

[9] Zhao, X., Wu, P., Lei, Y., Chen, F., Yu, Z., Fang, P., Liu, Y., 2020, Sun-light-driven plasmonic Ag/AgCl@TNT photocatalysts for high-efficient absorption-regeneration and photocatalytic degradation, *Appl. Surf. Sci.*, 529, 147010.

[10] Navidpour, A.H., Xu, B., Ahmed, M.B., and Zhou, J.L., 2024, Immobilization of TiO_2 and ZnO by facile surface engineering methods to improve semiconductor performance in photocatalytic wastewater treatment: A review, *Mater. Sci. Semicond. Process.*, 179, 108518.

[11] Constantino, D.S.M., Dias, M.M., Silva, A.M.T., Faria, J.L., and Silva, C.G., 2022, Intensification strategies for improving the performance of photocatalytic processes: A review, *J. Cleaner Prod.*, 340, 130800.

[12] Zheng, Z., He, J., Zhang, Z., Kumar, A., Khan, M., Lung, C.W., and Lo, I.M.C., 2024, Magnetically recyclable nanophotocatalysts in photocatalysis-involving processes for organic pollutant removal from wastewater: Current status and perspectives, *Environ. Sci.: Nano*, 11 (5), 1784–1816.

[13] Dhanalakshmi, R., Denardin, J.C., Sreekanth, T.V.M., Reddeppa, M., Rosaiah, P., Yoo, K., and Kim, J., 2023, Synergistic magnetic field-photocatalysis for the concurrent removal of inorganic and organic contaminants over $PrFeO_3$/ZnO heterostructures, *Inorg. Chem. Commun.*, 156, 111189.

[14] Zhang, D., Zuo, X., Gao, W., Huang, H., Zhang, H., Cong, T., Yang, S., Zhang, J., and Pan, L., 2022,

Recyclable ZnO/Fe_3O_4 nanocomposite with piezotronic effect for high performance photocatalysis, *Mater. Res. Bull.*, 148, 111677.

[15] Kaur, H., Singh, S., and Pal, B., 2023, Effect of plasmonic metal (Cu, Ag, and Au) loading over the physicochemical and photocatalytic properties of Mg-Al LDH towards degradation of tetracycline under LED light, *Appl. Surf. Sci.*, 609, 155455.

[16] Mu, F., Liu, C., Xie, Y., Zhou, S., Dai, B., Xia, D., Huang, H., Zhao, W., Sun, C., Kong, Y., and Leung, D.Y.C., 2021, Metal-organic framework-derived rodlike $AgCl/Ag/In_2O_3$: A plasmonic Z-scheme visible light photocatalyst, *Chem. Eng. J.*, 415, 129010.

[17] Wang, F., Liang, X., Wang, P., Zhang, Q., Tong, F., Wang, Z., Liu, Y., Zheng, Z., Cheng, H., Dai, Y., and Huang, B., 2021, Ag/AgCl as an efficient plasmonic photocatalyst for greenhouse gaseous methane oxidation, *J. Environ. Chem. Eng.*, 9 (6), 106435.

[18] Amir, M., Güner, S., Yıldız, A., and Baykal, A., 2017, Magneto-optical and catalytic properties of Fe_3O_4@HA@Ag magnetic nanocomposite, *J. Magn. Magn. Mater.*, 421, 462–471.

[19] Zhan, Y., Lan, J., Shang, J., Yang, L., Guan, X., Li, W., Chen, S., Qi, Y., and Lin, S., 2020, Durable ZIF-8/Ag/AgCl/TiO_2 decorated PAN nanofibers with high visible light photocatalytic and antibacterial activities for degradation of dyes, *J. Alloys Compd.*, 822, 153579.

[20] Wang, H., Shi, H., Li, H., Tian, X., Wu, Z., and Li, S., 2020, Decoration of Fe_3O_4 base material with Ag/AgCl nanoparticle as recyclable visible-light driven photocatalysts for highly-efficient photocatalytic disinfection of *Escherichia coli*, *Solid State Sci.*, 102, 106159.

[21] Lou, S., Chen, Q., Wang, W., Wang, Y., and Zhou, S., 2021, Template-assisted synthesis of Ag/AgCl hollow microcubes and their composition-dependent photocatalytic activity for the degradation of phenol, *RSC Adv.*, 11 (42), 26311–26318.

[22] Zhang, X., Shi, W., Wang, T., Wang, X., Li, C., and He, W., 2024, Investigation on the dual roles of pollutants adsorption on the catalyst surface during photocatalytic process, *J. Water Process Eng.*, 63, 105558.